RSC Advances

PAPER

Cite this: *RSC Adv.*, 2014, **4**, 31047

Hierarchical cystine flower based electrochemical genosensor for detection of *Escherichia coli* O157:H7†

Chandra Mouli Pandey,[ab] Ida Tiwari[b] and Gajjala Sumana*[a]

Received 13th May 2014
Accepted 23rd June 2014

DOI: 10.1039/c4ra04511d

www.rsc.org/advances

This work reports on a facile and reproducible approach to synthesize novel organic flowers of cystine (CysFls) with high uniformity. These 3D flower-like structures have a purely hierarchical arrangement, wherein each petal is composed of several cystine molecules with an average size of 50 μM, as determined by transmission electron microscopy. The CysFls were self-assembled onto a gold electrode and were utilized as matrices for the covalent immobilization of an *Escherichia coli* O157:H7 (*E. coli*) specific probe oligonucleotide that was identified from the 16s rRNA coding region of the *E. coli* genome. This fabricated CysFl platform sought to provide improved fundamental characteristics to electrode interface in terms of electro-active surface area and diffusion coefficient. Electrochemical impedance spectroscopy revealed that this genosensor exhibits a linear response to complementary DNA in the concentration range of 10^{-6} to 10^{-15} M with a detection limit of 1×10^{-15} M. Under optimal conditions, this genosensor was found to retain about 88% of its initial activity after being used for 6 times.

1. Introduction

Micro-organisms, such as bacteria and viruses, are widely found in food, soil, water and the intestinal tracts of humans and animals.[1] Some of these micro-organisms play a crucial role in nature, but some can have intense negative effects on both animals and humans.[2] Among them entero-hemorrhagic *Escherichia coli* (*E. coli* O157:H7) is a major food-borne and waterborne pathogen that causes diarrhea, hemorrhagic colitis, and hemolytic uremic syndrome.[3,4] The traditional methods reported for the detection of *E. coli* O157:H7 in food and water include cultures using selective media,[5] serotyping[6,7] and PCR amplification.[8,9] Although these methods exhibit high accuracy, but the operating procedure is complex, time consuming and some techniques even have limited sensitivity and specificity.[10] Hence, it is necessary to fabricate a sensitive, specific and rapid detection technique for *E. coli* which would have implications in environmental monitoring, food industry and clinical chemistry. Currently, surface plasmon resonance,[11] quartz crystal microbalance,[12] and electrochemical[13,14] transduction techniques have been proposed as substitutes to these conventional methods. Among them, electrochemical nucleic acid biosensing has attracted considerable interest because of its unique properties of simplicity, rapidity, accuracy, low cost and portability.[15,16] Electrochemical biosensors detect nucleic acid binding events on a solid-state transducer surface by monitoring electrochemical spectrum change.[16–18]

In the fabrication of high performance biosensors for clinical diagnostics, the structure and morphology of the matrices and the immobilization of bio-analytes for achieving rapid and sensitive detection of bio-recognition is a major challenge.[19] In view of the motivating phenomena occurring at ordered microstructures and nanoscale materials, significant work has recently been directed towards the synthesis of novel materials and exploring their applications in a variety of important fields including catalysis, point of care diagnostics for infectious diseases and therapeutics.[13,20,21] Presently, nanomaterials have been widely used as signal amplification mediums to enhance the limit of DNA detection.[22,23] In this context, the synthesis of polyaniline nanotubes has been reported that can detect nucleic acids with a detection limit of 1.0 fM.[24] The fabrication of a nanoporous gold electrode using encoded gold nanoparticles achieved a detection limit of about 28 aM.[25] A label-free DNA sensor has also been prepared using gallium nitride nanowires, revealing picomolar concentrations of target DNA.[26] Wang *et al.* have fabricated a gold nanoflower modified electrochemical DNA biosensor capable of detecting target DNA with a detection limit of 1 pM.[27] There are reports on the modification of electrodes by different nanomaterials to improve DNA detection but the strategies adopted for these modifications are relatively complex. The modification of the surface using surfactant or polymer matrix in the preparation and assembly of nanomaterials often causes some vague effects

[a]*Biomedical Instrumentation Section, CSIR-National Physical Laboratory, New Delhi-110012, India. E-mail: sumanagajjala@gmail.com; Tel: +91-11-45609152*

[b]*Department of Chemistry, Faculty of Science, Banaras Hindu University, Varanasi-221005, India*

† Electronic supplementary information (ESI) available. See DOI: 10.1039/c4ra04511d

in DNA detection.[28] Thus, it is necessary to develop a simple strategy for the construction of nanostructure modified electrodes for improved and sensitive detection of DNA. In this context, very few reports are available on the application of hierarchical structures of organic and related compounds for the fabrication of nucleic-acid biosensors. These hierarchically structured materials not only possess structural organization at various scales but they also lead to improved material properties and performance in terms of high surface area, synergistic interactions, and multiple functionalities.[29,30] Further, the ability to design these hierarchical structures from materials with self-assembling properties at the nanometer scale opens up new opportunities for application in the field of biosensors.[31,32]

Previously, we reported the detection of nucleic acids using micro-structured cystine dendrites, wherein the role of functional groups and the morphology of dendritic cystine were discussed.[33] However, there is a lot of scope in tailoring the order and morphology of the amino acid for enhancing the sensitivity and stability of the biosensor. Therefore, in the present work, detailed experiments have been carried out to explore the complexation efficiencies of the binding of DNA strands with probe molecules that are immobilized on cystine flowers (CysFls). These CysFls are being considered as model systems because of their intriguing properties such as the ease of preparation, less chemical handling, and they have a common functionality at one end of the molecule, which is coupled to a range of gradually differentiated functionalities at the other. Further, this CysFl has been utilized to fabricate a label free electrochemical genosensor by covalently immobilizing a specific probe oligonucleotide that is identified from the 16s rRNA coding region of the *E. coli* genome. This CysFl-based platform was found to possess increased electro-active surface area and high electron transport at the electrode–electrolyte interface, enhancing the sensitivity of the genosensor.

2. Materials and methods

2.1. Chemicals and oligonucleotides

L-Cysteine (analytical grade, 98.5%), *N*-hydroxysuccinimide (NHS), *N*-ethyl-*N*-(3-dimethylaminopropyl carbodiimide) (EDC), and all other reagents and solvents were procured from Sigma-Aldrich (India). Probe sequence specific to *E. coli* that identified from the 16s rRNA coding region of the *E. coli* genome, complementary, non-complementary and one-base mismatch target sequences were procured from Sigma Aldrich, Milwaukee, USA and are as follows:[13] DNA probe (pDNA): NH_2-5′-GGT CCG CTT GCT CTC GC-3′ complementary (cDNA): 5′-GCG AGA GCA AGC GGA CC-3′ non-complementary: 5′-CTA GTC GTA TAG TAG GC-3′ one-base mismatch: 5′-GCG AGA G*A*A AGC GGA CC-3′.

The bacterial culture samples of other water borne pathogens were provided by the All India Institute of Medical Sciences (AIIMS), New Delhi, India. The solutions of oligonucleotides were prepared in Tris–EDTA buffer (1 M Tris–HCl, 0.5 M EDTA) at pH 8.0 and stored at −20 °C prior to use.

2.2. Synthesis of cystine flowers (CysFls)

For the synthesis of the CysFls, 100 mM L-cysteine aqueous solution was prepared by maintaining the pH at 8.0 using sodium bicarbonate. The solution was sonicated for 30 min at 25 °C using an ultrasonic bath, and the crystal growth of the CysFls was observed by maintaining the solution at 25 °C for 12 h. For TEM analysis, the prepared CysFl was dropped onto a carbon grid and dried at room temperature.

2.3. Fabrication of CysFl/Au electrode

The gold (Au) electrode (0.5 cm^2 diameter) was washed in boiling 2.0 M aqueous KOH for about 1 h, followed by ultrasonication in piranha solution (3 : 1H_2SO_4–H_2O_2) for 10 min. The electrode was voltammetrically cycled and characterized in 0.2 M H_2SO_4 (−0.5 V to −1.4 V *vs.* Ag/AgCl) at a scan rate of 0.10 V s^{-1} until a stable cyclic voltammogram was obtained. The self-assembly of the CysFls was achieved by dipping a pre-cleaned gold electrode into 100 mM CysFl solution overnight (12 h) at 27 °C. After that, the electrodes were removed and washed repeatedly with de-ionized water.

2.4. Immobilization of probe DNA and hybridization with target DNA

The fabricated CysFl/Au electrode was activated using EDC (2 mM) and NHS (5 mM) and kept for 1 h in the dark. Subsequently, 40 μl of pDNA (10^{-6} M) was immobilized onto the modified electrode at 100% humidity at room temperature (~27 °C) for about 6 h, followed by rinsing with Tris–HCl. The hybridization studies were performed as a function of target DNA concentration with complementary, non-complementary and one-base mis-match sequences in a humid chamber for about 20 min at 35 °C. The proposed mechanism for the synthesis of a CysFl and the fabrication of the nucleic acid sensor for *E. coli* detection is shown in Scheme 1.

2.5. Extraction of DNA from bacterial clinical samples

The extraction of DNA was conducted from a panel of strains comprising *E. coli*, *Salmonella typhimurium*, *Neisseria meningitides*, and *Shigella dysenteriae*. For this process, the suspensions of the colonies were vortexed by pouring them into 100 μl of sterile MilliQ water. The suspension was boiled for 10 min and then centrifuged at 10 000 rpm for 5 min, followed by the addition of an equal volume (100 μl) of 24 : 1 (v/v) chloroform–iso-amyl alcohol. The solution was again centrifuged (12 000 rpm, 10 min), which resulted in the formation of an aqueous layer containing DNA which was carefully pipetted out and maintained at −20 °C prior to use.[33]

2.6. Pre-treatment of extracted DNA

All the bacterial clinical samples were prepared in Tris–EDTA buffer and were denatured by heating in a water bath (95 °C) for 5 min and were immediately chilled in ice to obtain the denatured single-stranded DNA. These aliquots of samples were subjected to sonication (15 min at 120 V) to break the long DNA strands into smaller fragments.[2]

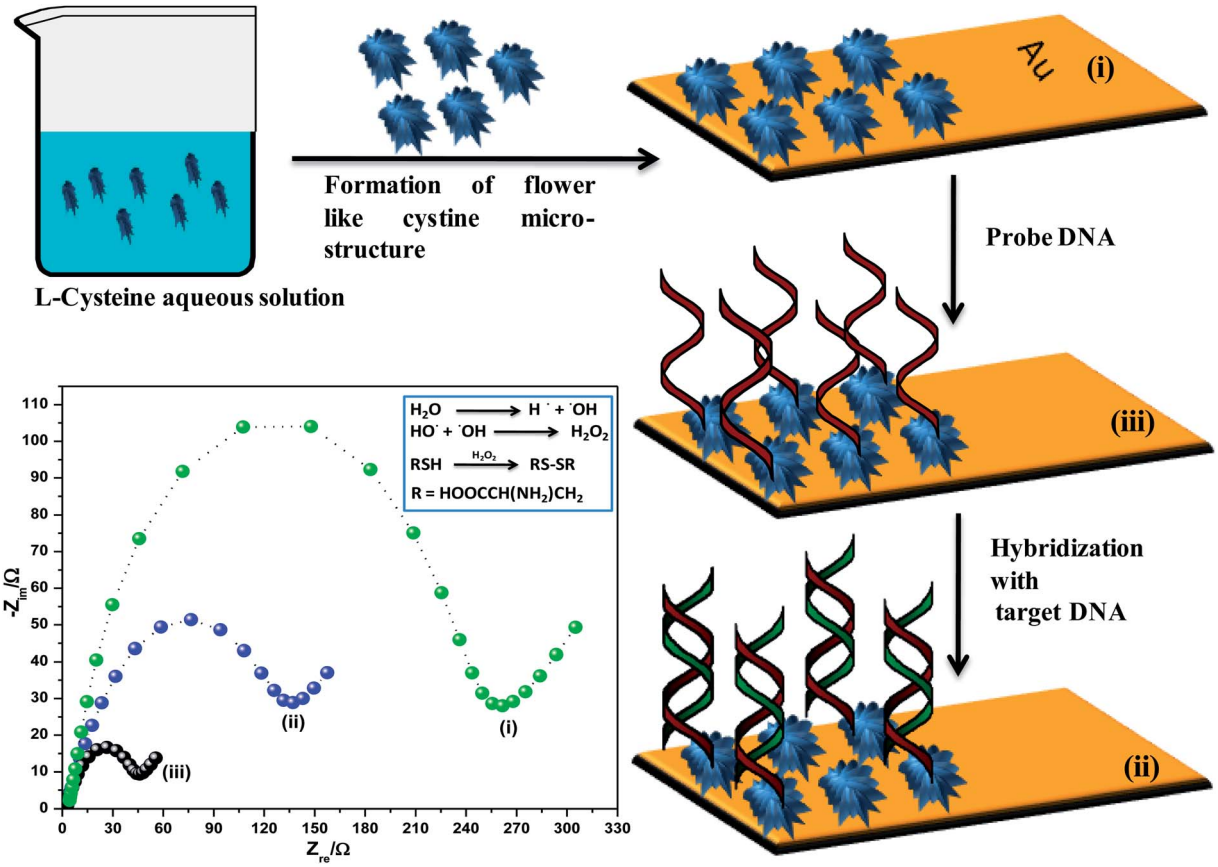

Scheme 1 Schematic showing the synthesis and fabrication of CysFl and the pDNA/CysFl/Au bioelectrode.

2.7. Characterization

The structural and morphological investigations of CysFl were carried out using X-ray diffraction (XRD, Cu Kα radiation, Rigaku, miniflax 2) and transmission electron microscopic (TEM, Hitachi Model, H-800) studies. The scanning electron microscopic (SEM) images were recorded using a JEOL-JSM-6700F field-emitting scanning electron microscope (FESEM, 15 kV). Contact angle (CA) measurements were obtained using a contact angle meter (Data Physics OCA15EC). Fourier transform infra-red (FT-IR) spectroscopy measurements were carried out using a Perkin-Elmer spectrometer (Model Spectrum BX) at 25 °C. Electrochemical analysis was carried out on an Autolab potentiostat/galvanostat (Eco Chemie, Netherlands) using a three-electrode cell with Au as the working electrode, platinum as the auxiliary electrode and Ag/AgCl as the reference electrode in phosphate buffer saline (PBS, 100 mM, pH 7.0, 0.9% NaCl) containing 5 mM $[Fe(CN)_6]^{3-/4-}$.

3. Results and discussion

3.1. Characterization of CysFl

The powder XRD pattern of CysFl is displayed in Fig. 1A. The main diffraction peaks of the CysFl structures appear at 18.8°, 28.4°, 33.0° and 34.3° corresponding to 100, 001, 112, and 116, respectively. The diffraction peaks show a pure hexagonal phase, which is in good agreement with the standard value for bulk hexagonal L-cystine (JCPDS 261776).[33,34] FTIR spectroscopy was used to characterize CysFl and the pDNA/CysFl/Au electrode in the frequency region of 400–1800 cm^{-1}. The characteristic bands of CysFl seen at 1490 cm^{-1} are attributed to the presence of amino groups. Intense absorption peaks at 1590 cm^{-1}, 1624 cm^{-1} and 1420 cm^{-1}, 1490 cm^{-1} may be assigned to the asymmetric deformation of NH_3^+ and the asymmetric stretching of COO^-, respectively. Bands observed at 1420 cm^{-1}, 1295 cm^{-1} and 782 cm^{-1} are attributed to CH_2–CO deformation, CH_2 wagging and rocking vibrations, respectively, confirming the presence of CH_2 groups (Fig. 1B).[32,33] After the immobilization of pDNA on CysFl, the nitrogen base region (1700–1500 cm^{-1}) in the DNA spectrum overlaps with the amine signals of CysFl. The absorption bands seen at 1330 and 1133 cm^{-1} may be attributed to the anti-symmetric and symmetric stretching vibrations of the phosphate groups, respectively (Fig. 1C). Further, the IR absorption peak at 1048 cm^{-1} is because of the vibration of ribose (C–C sugar), and the absorption at 903 cm^{-1} is an indication of the immobilization of DNA on the surface of CysFl.

3.2. Microscopic analysis of the CysFl

TEM studies have been carried out to study the formation of CysFl. Fig. 2A shows that the CysFl consists of several hexagonal

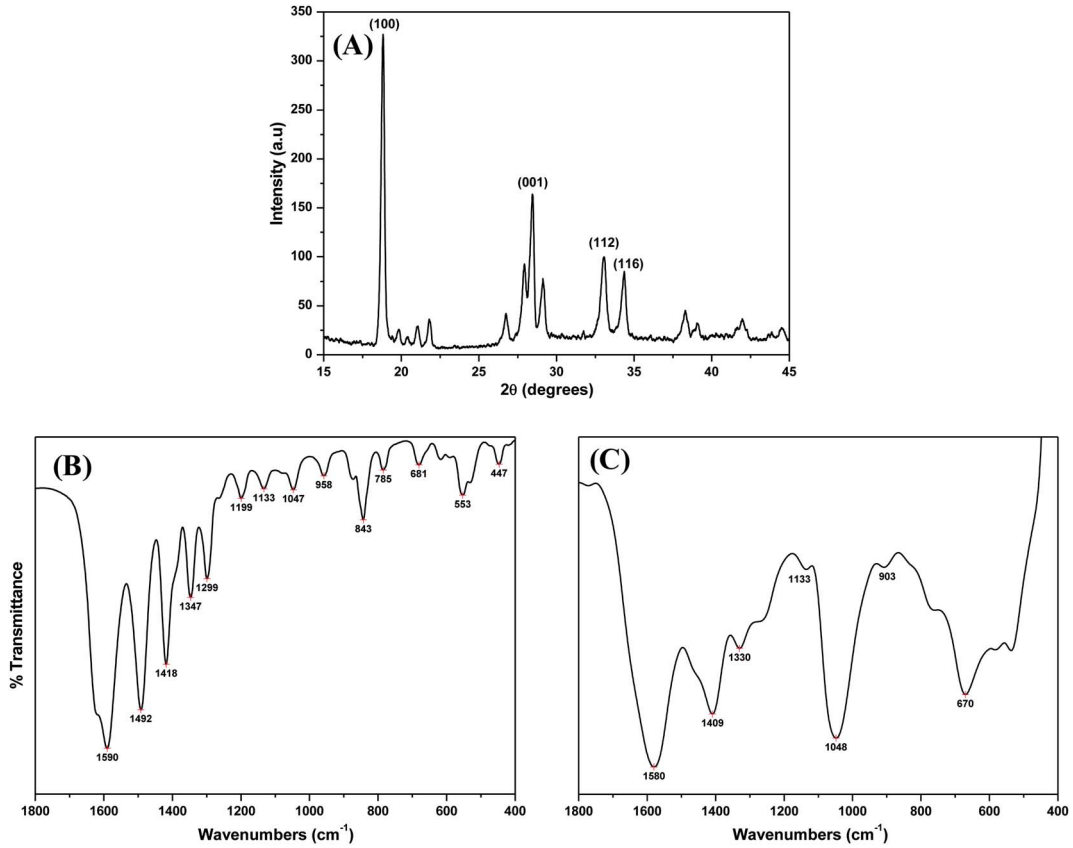

Fig. 1 (A) X-ray diffraction pattern of CysFl. FT-IR spectra of (B) CysFl/Au electrode, and (C) pDNA/CysFl/Au bioelectrode.

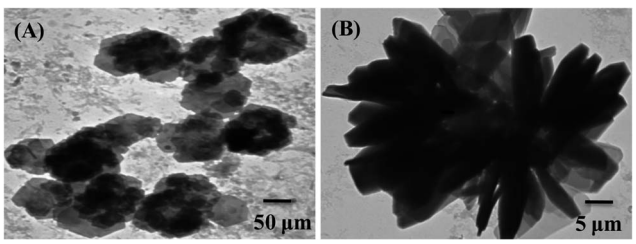

Fig. 2 TEM image showing (A) the formed CysFl at pH 8.0 and 100 mM concentration and (B) the arrangement of hexagonal petals in CysFl.

structures arranged in an ornate manner, where the size of each flower is 50 μM. High resolution TEM images show that the thickness of each hexagonal flake is about 1 μM (Fig. 2B) and they are arranged facial to each other. TEM studies reveal that the growth of these CysFls start with the formation of cystine hexagons, and with an increase in the reaction time these primary hexagonal cystine crystals agglomerate and result in the formation of flower-like structures.[32] The formation of these structures can be attributed to acoustic cavitations, and the mechanism is described elsewhere.[33] It appears that the intermolecular electrostatic interactions of hydrogen bonding are responsible for the formation of CysFl, which depends on the change in pH.[35]

3.3. Morphological characterization of the CysFl/Au and pDNA/CysFl/Au electrodes

The surface morphological studies of the CysFl/Au and DNA/CysFl/Au bioelectrodes were investigated using SEM. Fig. 3A shows the self-assembly of CysFl onto gold surface, where the assemblies are formed in isolation and are not connected. The high magnification image shows that each flower consists of several hexagonal flakes arranged in a patterned manner (Fig. 3A, inset). After the immobilization of pDNA on the CysFl/Au electrode, a shiny morphology is observed (Fig. 3B), showing the complete coverage of CysFls by pDNA. This increase in the chemically accessible area may be due to well-oriented functional groups present in the CysFl which help in the covalent binding of the amino terminated pDNA.

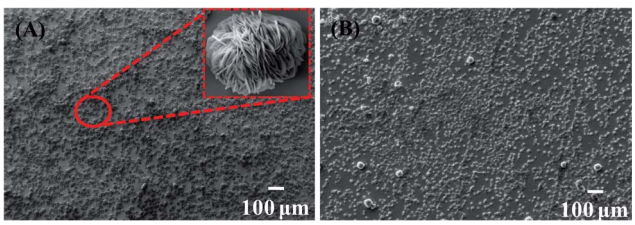

Fig. 3 SEM image of (A) CysFl/Au electrode, and (B) pDNA/CysFl/Au bioelectrode.

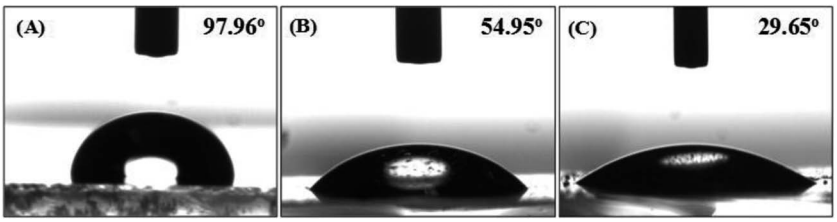

Fig. 4 Contact angle measurements of (A) Au electrode, (B) CysFl/Au electrode, and (C) pDNA/CysFl/Au bioelectrode.

3.4. Contact angle (CA) studies for Au, CysFl/Au and pDNA/CysFl/Au electrodes

To investigate the immobilization of pDNA onto CysFl/Au electrode, CA measurements were carried out using the sessile drop method. The change in contact angle reveals the hydrophobic/hydrophilic character of the surface, which in turn can be related to CysFl self-assembly and pDNA immobilization on the CysFl/Au electrode. Table S1† shows the CA data of bare Au, CysFl/Au and pDNA/CysFl/Au bioelectrodes. It can be seen that the value of CA decreases after the self-assembly of CysFl (Fig. 4B) onto the Au electrode (Fig. 4A), indicating the presence of numerous hydrophilic functional groups (–COOH, $–NH_2$ and –SH) in CysFl. CA measurements were also performed to confirm the immobilization of pDNA onto the CysFl/Au electrode, and it was found that with the progress of the immobilization process, the surface becomes more hydrophilic because of the presence of the phosphodiester backbone of pDNA. The CA value subsequently decreases with time (4–18 h) and becomes constant at 29.65° (Fig. 4C) after about 6 h revealing that the complete immobilization of the probe occurs in this time frame.

3.5. Electrochemical characterization

3.5.1. Electrochemical impedance spectroscopy studies. Electrochemical impedance spectroscopy (EIS) is a powerful and sensitive tool for studying the charge transfer processes occurring at the electrode-solution or modified electrode-solution interfaces.[36] In the Nyquist plot of impedance spectra, the semicircle corresponds to the electron transfer resistance process (R_{ct}), which usually depends on the dielectric and insulating features at the electrode–electrolyte interface.[37,38]

Fig. 5 shows the EIS studies of the CysFl/Au electrode, EDC/NHS activated CysFl/Au electrode and pDNA/CysFl/Au bioelectrode in phosphate buffer (100 mM, pH 7.0, 0.9% NaCl) containing 5 mM $[Fe(CN)_6]^{3-/4-}$ as a redox marker. The equivalent circuit (Fig. 5, inset) and the calculated values for solution resistance (R_s), constant phase element (C_{PE}), and warburg impedance (W) value, corresponding to different modifications are given in Table S2.† In the impedance spectra, the low frequency semi-circle is the characteristic of an interfacial charge transfer reaction. The surface modification of the Au electrode with CysFl results in an increase of the R_{ct} value (250.4 Ω, curve (i)). This increase in the R_{ct} value is because of the presence of negative charges from the $–COO^-$ groups of CysFl that interrupt the interfacial electron-transfer rate between the electrode and the electrolyte solution. Interestingly, when the CysFl/Au electrode was activated with EDC/NHS, there was a decrease in the R_{ct} value, which may be attributed to the blocking of the negative charges of the $–COO^-$ groups of CysFl, and the available net positive charges attract negative redox markers, resulting in the decrease of R_{ct} (16.7 Ω, curve (iv)).[33] When the pDNA was immobilized on the CysFl/Au electrode there was an increase in the R_{ct} value (47.54 Ω, curve (iii)) that could be attributed to the repellence of the redox probe from the approaching electrode surface by the negatively charged phosphate skeletons of DNA. Further, when the pDNA is incubated with its cDNA sequence, hybridization occurs and more negatively charged phosphate backbones are introduced, resulting in an increase of R_{ct} (149.3 Ω, curve (ii)).

3.5.2. Cyclic voltammetry studies. To investigate various kinetic parameters, the cyclic voltammograms of the pDNA/CysFl/Au electrode were recorded as a function of scan rate (10–300 mV s^{-1}). It was observed that the magnitude of the electrochemical response current [anodic (I_{pa}) and cathodic (I_{pc}), Fig. S1A†] for the bioelectrodes is linearly dependent on the scan rate and follows eqn (1) and (2). The separation of the peaks suggests that the process is not perfectly reversible;

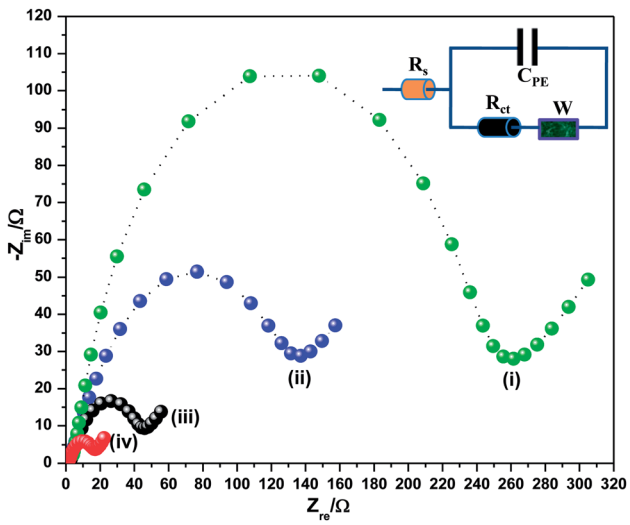

Fig. 5 EIS showing the Nyquist diagram (Z_{im} *versus* Z_{re}) for Faradic impedance measured in 5 mM $[Fe(CN)_6]^{3-/4-}$ PBS solution at pH 7.0 at frequency ranging from 10^5 Hz to 0.1 Hz (i) CysFl/Au electrode (ii) complementary DNA incubated on pDNA/CysFl/Au bioelectrode (iii) pDNA/CysFl/Au bioelectrode (iv) EDC/NHS activated CysFl/Au electrode.

however, stable redox peak current and position during repeated scans at a particular scan rate suggests that CysFl-based electrodes exhibit a quasi-reversible process.[37] It was also observed that the magnitude of both anodic (E_a) and cathodic peak (E_c) potentials (Fig. S1B†) increases linearly as a function of scan rate (eqn (3) and (4)), which reveals that electron transport from redox moieties to the electrode is very facile.

$$I_{pa}\,(A)\,[pDNA/CysFl/Au] = 4.8957 \times 10^{-5}\,(A) + 5.3112 \times 10^{-5}\,A\,(s\,mV^{-1})\,[scan\ rate\ (mV\ s^{-1})]\ R = 0.9986,\ SD = 1.208 \times 10^{-5} \quad (1)$$

$$I_{pc}\,(A)\,[pDNA/CysFl/Au] = -1.1785 \times 10^{-4}\,(A) - 3.542 \times 10^{-5}\,A\,(s\,mV^{-1})\,[scan\ rate\ (mV\ s^{-1})]\ R = 0.9920,\ SD = 1.8612 \times 10^{-5} \quad (2)$$

$$E_a\,(V)\,[pDNA/CysFl/Au] = 0.1302\,(V) + 0.4606\,(V) \times \log[scan\ rate]\ R = 0.9776,\ SD = 0.0043 \quad (3)$$

$$E_c\,(V)\,[pDNA/CysFl/Au] = 0.1181\,(V) - 0.0384\,(V) \times \log[scan\ rate]\ R = 0.9885,\ SD = 0.0025 \quad (4)$$

On the basis of the linear slope of anodic peak currents on the square root of potential sweep rates (Fig. S1B†), it is clear that ion transport from the bulk to the electrode surface occurs exclusively by diffusion.[39] Further, the diffusion coefficient is calculated by a concentration gradient of $[Fe(CN)_6]^{3-/4-}$ ions between the bulk and the interface, which can be calculated using the Randles–Sevick equation:

$$I_p = (2.99 \times 10^5)\alpha^{1/2}n^{3/2}ACD^{1/2}\nu^{1/2} \quad (5)$$

The diffusion coefficient for the pDNA/CysFl/Au electrode is calculated to be 7.19×10^{-6} cm^2 s^{-1} and for the CysFl/Au electrode it was found to be 1.02×10^{-5} cm^2 s^{-1}. From the abovementioned kinetics calculation it can be inferred that the CysFl/Au assembly is expected to provide improved electron transfer kinetics to the electrode interface.

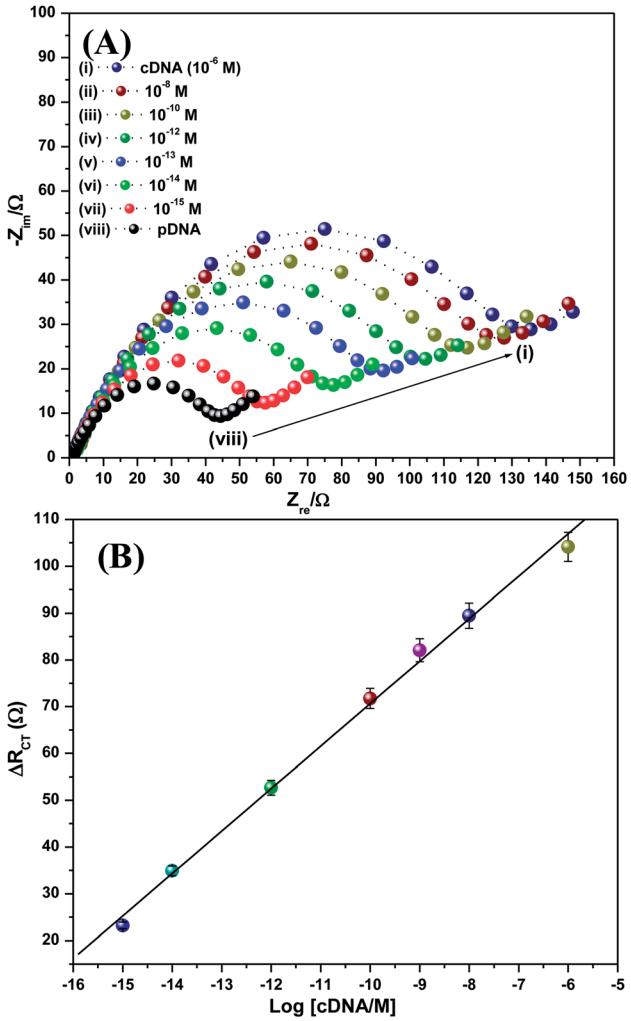

Fig. 6 EIS response of (A) pDNA/CysFl/Au bioelectrode as a function of cDNA concentration (10^{-6} to 10^{-15} M) in 5 mM $[Fe(CN)_6]^{3-/4-}$ PBS solution at pH 7.0. (B) Plot of the ratio of charge transfer resistance after and before hybridization, R_{ct} target/R_{ct} pDNA of the pDNA/CysFl/Au bioelectrode *vs.* the logarithm of target DNA concentrations.

3.6. Electrochemical response studies

3.6.1. Response studies of the pDNA/CysFl/Au bioelectrode. The sensitivity of the pDNA/CysFl/Au bioelectrode was investigated using EIS by varying the cDNA concentration from 10^{-6} M to 10^{-15} M (Fig. 6A). It was found that with the change in cDNA concentration, there was a change in the R_{ct} value. This signifies that the hybridization reaction is occurring at the bioelectrode because of which there is increased accumulation of negatively charged phosphate backbones; hence, the R_{ct} value increases with the formation of double stranded DNA. The difference ($\Delta R_{ct} = R_{ct(cDNA)} - R_{ct(pDNA)}$) between the value of the pDNA immobilized electrode and that after hybridization with cDNA has been used as the measurement signal. The analytical signal (ΔR_{ct}) shows a linear relationship with the logarithmic value of complementary target DNA concentration ranging from 10^{-15} to 10^{-6} M (Fig. 6B) and follows eqn (6):

$$\Delta R_{ct} = 161.47 + 9.07 \log cDNA \quad (6)$$

with a linear regression coefficient of 0.998. The detection limit was calculated to be 1×10^{-15} M using the expression 3σ, where σ was estimated as the standard deviation ($n = 10$) of the impedimetric signals obtained in the absence of bacteria. As the CysFls contain ample functional groups for the immobilization of biomolecules, a higher quantity of pDNA is immobilized onto the CysFl/Au electrode, leading to an enhancement in hybridization efficiency. In this case, the pathway of electron transfer to/from the electrode was very effectively blocked and the changes in the R_{ct} values were remarkably enhanced upon hybridization, leading to a low detection limit. Further, the association constant (K_a) between cDNA and the pDNA/CysNf/Au bioelectrode was estimated from the slope of regression equation and was found to be 0.243 M^{-1} (Fig. S2†).[40,41] The performance of the DNA hybridization detection based on the pDNA/CysFl/Au platform were compared with other hierarchical structure-based biosensors, as shown in Table 1. It was

Table 1 Performances of the DNA hybridization detection based on pDNA/CysFl/Au platform compared with other hierarchical structure based platform

Sl. no	Immobilization matrix	Transducer used	Detection limit	Detection range	Reusability	Stability	Ref.
1	Au nanoflower	DPV	1×10^{-12} M	1×10^{-12} to 0.1×10^{-6} M	8 times (15% loss of original signal)	2 weeks (86% of initial response	27
2	Polyaniline nanofibers/ flower-like Au microsphere	EIS	1.9×10^{-14} M	1×10^{-13} to 1×10^{-6} M	6 times (with standard deviation of 3.05%)	10 days (94% of its initial response)	42
3	Au nanoparticle decorated graphene sheets	EIS	3.4×10^{-14} M	1×10^{-13} to 1×10^{-6} M	3 times (loss of original signal 6.04%)	—	43
4	Polyaniline nanotube	DPV	1.9×10^{-15} M	3.5×10^{-15} to 755.7×10^{-15} M	2 times (with standard deviation of 3%)	—	24
5	Dendritic cystine/Au	EIS	0.1×10^{-13} M	1×10^{-14} to 1×10^{-6} M	4 times (signal loss not mentioned)	4 weeks	33
6	Cystine nanoflower/Au	EIS	1×10^{-15} M	1×10^{-15} to 1×10^{-6} M	6 times (10.37% signal loss)	30 days (90% of its initial response)	Present work

observed that the CysFl-based platform has a lower detection limit and a wider detection range for nucleic acids.

3.7. Selectivity of the bioelectrode

The specificity of the pDNA/CysFl/Au bioelectrode towards different target DNA sequences (complementary, non-complementary and one base mismatch) and culture samples of *E. coli*, *S. typhimurium*, *N. meningitidis* and *S. dysenteriae* was studied using EIS (Fig. 7). After the incubation of bioelectrode with *E. coli* spiked and *E. coli* culture DNA, there was a marked increase in the semicircle diameter; the R_{ct} value was nearly the same as that of cDNA, confirming the process of hybridization. When the pDNA/CysFl/Au bioelectrode was incubated with non-complementary and culture samples of bacterial pathogens DNA, there was a slight or negligible change in the R_{ct} value with respect to pDNA. Because the non-complementary DNA bases do not match with the pDNA bases, it was expected that no hybridization occurs, and the R_{ct} should result in a semicircle diameter similar to that of the pDNA/CysFl/Au bioelectrode (Fig. 7, inset).[33] A slight increase in R_{ct} for *S. typhimurium* and *N. meningitidis* DNA was observed, which may be because of nonspecific DNA interactions with the pDNA/CysFl/Au bioelectrode surface, leading to an increase in negative charges on the electrode surface. When the pDNA/CysFl/Au bioelectrode was exposed to the one base mis-match DNA sequence, there was a slight increase in the semicircle diameter in comparison to that of the pDNA. This may be because of the partial hybridization of pDNA with the complementary bases of the one base mis-match DNA, resulting in increased negative charge of the electrode surface due to the higher blocking effect of the surface or the repulsion of the marker ion.[19] These results reveal that the fabricated genosensor based on the CysFl/Au platform is highly specific for the detection of *E. coli* O157:H7.

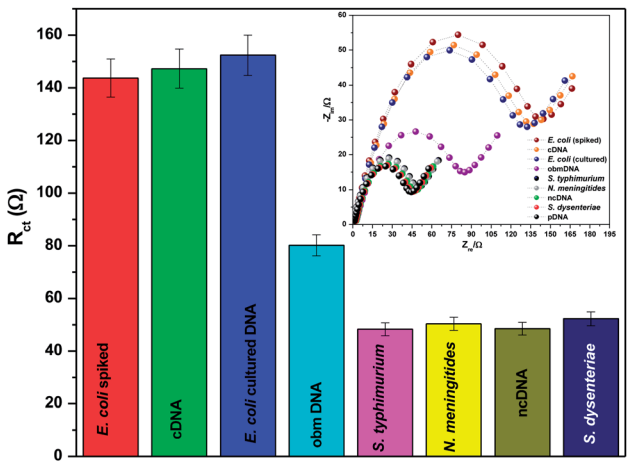

Fig. 7 Bar diagram showing the change in R_{ct} values for (i) spiked *E. coli* (ii) cDNA (iii) *E. coli* cultured (ii) one base mismatch (iii) *S. typhimurium* (iv) *N. meningitidis* (v) non complementary (iv) *S. dysenteriae* immobilized onto (v) pDNA/CysFl/Au bioelectrode. Inset figure shows the Nyquist plots for different cultured sample immobilized onto pDNA/CysFl/Au bioelectrode in 5 mM $[Fe(CN)_6]^{3-/4-}$ PBS solution at pH 7.0.

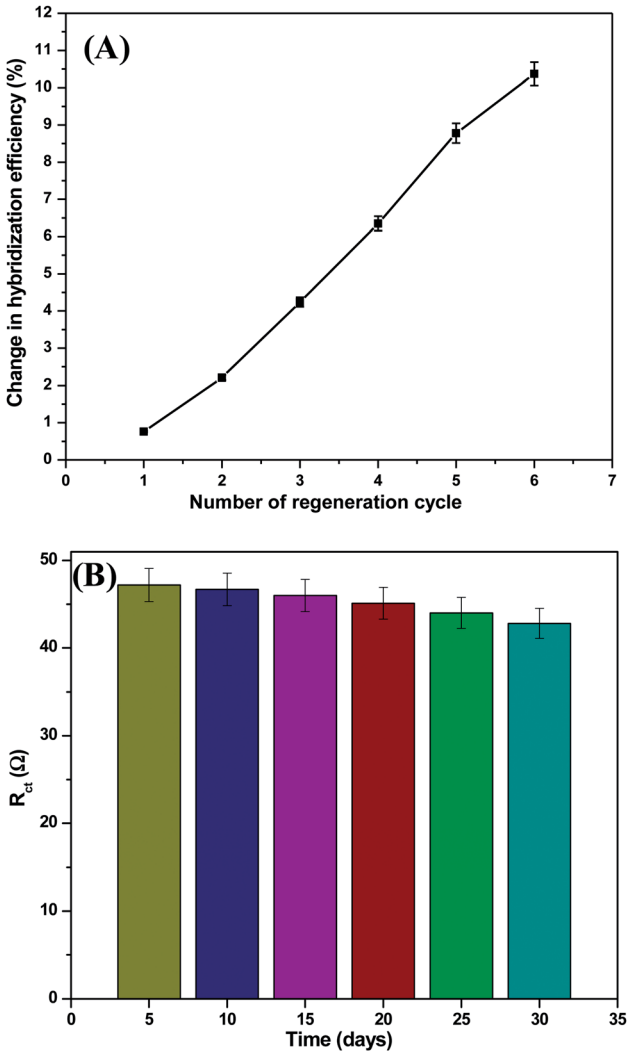

Fig. 8 (A) Percentage change in the R_{ct} of the fabricated pDNA/CysFl/Au bioelectrode towards *E. coli* detection was determined after each regeneration cycle (6 cycles). (B) Bar diagram showing the stability of the fabricated pDNA/CysFl/Au bioelectrode.

3.8. Reusability and stability of the bioelectrode

The strong binding of pDNA with the CysFl/Au electrode surface shows the stability of the genosensor to allow ready regeneration. For this, the electrode was immersed in a buffer solution (pH 8.0) containing Tris–HCl (10 mM) and EDTA (1 mM) at 100 °C for 5 min, followed by cooling in an ice bath for about 30 min, which completely removed cDNA *via* thermal denaturation.[39] The R_{ct} value of the genosensor was found to decrease after each regeneration process with an average signal loss of about 2% (Table S3†). This reduction in signal may be due to surface fouling during the regeneration process. The total loss of hybridization signal after 6 cycles is about 15.4 Ω, which corresponds to ~11.37% loss of the initial value, indicating that the bioelectrode reproducibly detects target DNA with repeated uses (Fig. 8A). To investigate the storage stability of the fabricated sensor, five measurements were recorded each week for over 30 days of continuous analysis. The decrease in signal response of the bioelectrode observed was less than 10% when it was stored at 4 °C (Fig. 8B).

4. Conclusions

In summary, the present work emphasizes the synthesis of cystine flowers prepared using the acoustic cavitation method and their application for *E. coli* detection. The structural and morphological studies provided strong evidence for the formation of CysFl and its self-assembly onto a gold electrode. Label-free detection using an electrochemical impedance spectroscopic technique reveals that the fabricated biosensor with an appropriately optimized protocol can accurately detect *E. coli* in the range of 10^{-6} to 10^{-15} M. This fabricated biosensor was found to be selective for *E. coli* detection and retains significant amount of activity (88% of the initial activity) after using for 6 cycles. Our sensing strategy could be extended for the detection of other micro-organisms and open up new avenues for the designing of electrochemical nucleic acid sensors.

Acknowledgements

We thank Prof. R.C. Budhani, Director, CSIR-NPL, New Delhi, India for the facilities. C.M.P. is thankful to CSIR, India, for the award of SRF. We thank Dr A.M. Biradar (NPL, New Delhi), Prof. B.D. Malhotra (DTU, Delhi) and Dr A.K. Pandey (PGIMER, Chandigarh) for interesting discussions. Thanks are due to Dr Seema Sood (AIIMS, New Delhi) for providing the bacterial culture samples. The financial support received from DST, (Grant no. DST/TSG/ME/2008/18) India is gratefully acknowledged.

References

1 P. Leonard, S. Hearty, J. Brennan, L. Dunne, J. Quinn, T. Chakraborty and R. O'Kennedy, *Enzyme Microb. Technol.*, 2003, **32**, 3–13.
2 C. M. Pandey, R. Singh, G. Sumana, M. K. Pandey and B. D. Malhotra, *Sens. Actuators, B*, 2011, **151**, 333–340.
3 H. Karch, P. I. Tarr and M. Bielaszewska, *Int. J. Med. Microbiol.*, 2005, **295**, 405–418.
4 J. G. Wells, B. R. Davis, I. K. Wachsmuth, L. W. Riley, R. S. Remis, R. Sokolow and G. K. Morris, *J. Clin. Microbiol.*, 1983, **18**, 512–520.
5 T. S. Hammack, P. Feng, R. M. Amaguana, G. A. June, P. S. Sherrod and W. H. Andrews, *J. AOAC Int.*, 1997, **80**, 335–340.
6 P. A. Chapman, A. T. Malo, C. A. Siddons and M. Harkin, *Appl. Environ. Microbiol.*, 1997, **63**, 2549–2553.
7 J. Czajka and C. A. Batt, *J. Appl. Microbiol.*, 1996, **81**, 601–607.
8 J. A. Higgins, S. Nasarabadi, J. S. Karns, D. R. Shelton, M. Cooper, A. Gbakima and R. P. Koopman, *Biosens. Bioelectron.*, 2003, **18**, 1115–1123.
9 G. Wang, C. G. Clark and F. G. Rodgers, *J. Clin. Microbiol.*, 2002, **40**, 3613–3619.

10 X. Jiang, K. Chen, J. Wang, K. Shao, T. Fu, F. Shao, D. Lu, J. Liang, M. F. Foda and H. Han, *Analyst*, 2013, **138**, 3388–3393.
11 A. D. Taylor, Q. Yu, S. Chen, J. Ã. Homola and S. Jiang, *Sens. Actuators, B*, 2005, **107**, 202–208.
12 X. Mao, L. Yang, X.-L. Su and Y. Li, *Biosens. Bioelectron.*, 2006, **21**, 1178–1185.
13 C. M. Pandey, A. Sharma, G. Sumana, I. Tiwari and B. D. Malhotra, *Nanoscale*, 2013, **5**, 3800–3807.
14 P. Geng, X. Zhang, Y. Teng, Y. Fu, L. Xu, M. Xu, L. Jin and W. Zhang, *Biosens. Bioelectron.*, 2011, **26**, 3325–3330.
15 N. Prabhakar, K. Arora, S. K. Arya, P. R. Solanki, M. Iwamoto, H. Singh and B. D. Malhotra, *Analyst*, 2008, **133**, 1587–1592.
16 J. Wang, *Anal. Chim. Acta*, 2002, **469**, 63–71.
17 A. Bonanni and M. del Valle, *Anal. Chim. Acta*, 2010, **678**, 7–17.
18 C.-z. Li, H. Karadeniz, E. Canavar and A. Erdem, *Electrochim. Acta*, 2012, **82**, 137–142.
19 B. Chen, Y. Xiao, C. Liu, C. Li and F. Leng, *Nucleic Acids Res.*, 2010, **38**, 3643–3654.
20 J. Wang, G. Rivas, X. Cai, M. Chicharro, C. Parrado, N. Dontha, A. Begleiter, M. Mowat, E. Palecek and P. E. Nielsen, *Anal. Chim. Acta*, 1997, **344**, 111–118.
21 P. Wagner, M. Hegner, P. Kernen, F. Zaugg and G. Semenza, *Biophys. J.*, 1996, **70**, 2052–2066.
22 J. Wang, *Anal. Chim. Acta*, 2003, **500**, 247–257.
23 A. Erdem, *Talanta*, 2007, **74**, 318–325.
24 H. Chang, Y. Yuan, N. Shi and Y. Guan, *Anal. Chem.*, 2007, **79**, 5111–5115.
25 K. Hu, D. Lan, X. Li and S. Zhang, *Anal. Chem.*, 2008, **80**, 9124–9130.
26 C.-P. Chen, A. Ganguly, C.-H. Wang, C.-W. Hsu, S. Chattopadhyay, Y.-K. Hsu, Y.-C. Chang, K.-H. Chen and L.-C. Chen, *Anal. Chem.*, 2008, **81**, 36–42.
27 L. Wang, X. Chen, X. Wang, X. Han, S. Liu and C. Zhao, *Biosens. Bioelectron.*, 2011, **30**, 151–157.
28 N. Singh, B. Manshian, G. J. S. Jenkins, S. M. Griffiths, P. M. Williams, T. G. G. Maffeis, C. J. Wright and S. H. Doak, *Biomaterials*, 2009, **30**, 3891–3914.
29 Z. Ren, Y. Guo, C.-H. Liu and P.-X. Gao, *Front. Chem.*, 2013, **1**, 18.
30 M. Byun, N. B. Bowden and Z. Lin, *Nano Lett.*, 2010, **10**, 3111–3117.
31 Y.-P. Zhu, T.-Z. Ren, T.-Y. Ma and Z.-Y. Yuan, *Int J Photoenergy*, 2014, **2014**, 15.
32 C. M. Pandey, G. Sumana and I. Tiwari, *Biosens. Bioelectron.*, 2014, **61**, 328–335.
33 C. M. Pandey, G. Sumana and B. D. Malhotra, *Biomacromolecules*, 2011, **12**, 2925–2932.
34 J. D. Rimer, Z. An, Z. Zhu, M. H. Lee, D. S. Goldfarb, J. A. Wesson and M. D. Ward, *Science*, 2010, **330**, 337–341.
35 H. Hongliang, W. Chungang, M. Zhanfang and S. Zhongmin, *Nanotechnology*, 2006, **17**, 5163.
36 F. Lisdat and D. Schäfer, *Anal. Bioanal. Chem.*, 2008, **391**, 1555–1567.
37 A. Kaushik, A. Vasudev, S. K. Arya and S. Bhansali, *Biosens. Bioelectron.*, 2013, **50**, 35–41.
38 A. Kaushik, P. R. Solanki, K. Kaneto, C. G. Kim, S. Ahmad and B. D. Malhotra, *Electroanalysis*, 2010, **22**, 1045–1055.
39 A. Sharma, G. Sumana, S. Sapra and B. D. Malhotra, *Langmuir*, 2013, **29**, 8753–8762.
40 I. Szymanska, H. Radecka, J. Radecki and R. Kaliszan, *Biosens. Bioelectron.*, 2007, **22**, 1955–1960.
41 S. K. Arya, T. S. Pui, C. C. Wong, S. Kumar and A. R. A. Rahman, *Langmuir*, 2013, **29**, 6770–6777.
42 X. Wang, T. Yang, X. Li and K. Jiao, *Biosens. Bioelectron.*, 2011, **26**, 2953–2959.
43 Y. Hu, S. Hua, F. Li, Y. Jiang, X. Bai, D. Li and L. Niu, *Biosens. Bioelectron.*, 2011, **26**, 4355–4361.